

Persistent plasma waves in interstellar space detected by Voyager 1

Stella Koch Ocker^{1,*}, James M. Cordes¹, Shami Chatterjee¹, Donald A. Gurnett², William S. Kurth², and Steven R. Spangler²

¹Department of Astronomy and Cornell Center for Astrophysics and Planetary Science, Cornell University, Ithaca, NY 14850, USA

²Department of Physics and Astronomy, University of Iowa, Iowa City, IA 52242, USA

*sko36@cornell.edu

In 2012, Voyager 1 became the first in situ probe of the very local interstellar medium¹. The Voyager 1 Plasma Wave System has given point estimates of the plasma density spanning about 30 astronomical units (au) of interstellar space, revealing a large-scale density gradient^{2,3} and compressive turbulence⁴ outside the heliopause. Previous studies of the plasma density relied exclusively on the detection of discrete plasma oscillation events that are triggered ahead of shocks propagating outwards from the Sun, and that can be used to infer the plasma frequency and hence density^{5,6}. We present the detection of a new class of very weak, narrowband plasma wave emission in the Voyager 1 Plasma Wave System data that persists from 2017 onwards and enables the first steadily sampled measurement of the interstellar plasma density over about 10 au with an average sampling time of 3 days, or 0.03 au. We find au-scale density fluctuations that trace turbulence in the interstellar medium between episodes of previously detected plasma oscillations. Possible mechanisms for the narrowband emission include thermally excited plasma oscillations and quasi-thermal noise, and could be clarified by new findings from Voyager or a future interstellar mission. The persistence of the emission suggests that Voyager 1 may be able to continue tracking the interstellar plasma density in the absence of shock-generated plasma oscillation events.

Since crossing the heliopause, Voyager 1 (V1) has measured the plasma density of the very local interstellar medium (VLISM) by detecting plasma oscillation events (POEs). The Plasma Wave System (PWS) measures these POEs as narrow (≈ 0.2 to 0.4 kHz wide) features in frequency-time spectra obtained with the wideband receiver and the plasma wave spectrometer. Fig. 1 is a composite dynamic spectrum showing all of the high-time resolution data available from the PWS wideband receiver since V1 crossed the heliopause until early 2020. The wideband receiver measures the voltage difference at the antenna terminals at a rate of $28,800$ samples s^{-1} , which is converted into a frequency-time dynamic spectrum by Fourier transforming the voltage time series. The resulting spectrum shows the relative electric field intensity for frequencies up to 10 kHz, the frequency roll-off imposed by the low-pass filter on the receiver. The composite spectrum in Fig. 1 shows salient features between 1.9 and 3.5 kHz and has time and frequency resolutions of 3 days and 0.011 kHz, respectively (see Methods).

About eight distinct POEs are visible in the composite dynamic spectrum beginning in late 2012. While the duration of these events ranges from a couple of days to about a year, they are all believed to be generated via beam-plasma instabilities in the electron foreshocks of shocks propagating out of the heliosphere⁶. The POEs share some key characteristics, including: 1) a spreading in frequency associated with the excitation of higher wave modes via, e.g., Langmuir parametric decay e.g.,^{7,8}; 2) an upward frequency drift attributed to the increase in plasma density as the shock propagates over the spacecraft, which in two cases has been directly associated with a jump in magnetic field strength characteristic of a quasi-perpendicular shock^{5,9,10}; and 3) fast (\sim sub-second level) intensity variations accompanied by smoother, broadband radio emission generated in a nonlinear mode conversion process. Most of these events are preceded by relativistic cosmic ray bursts detected by the V1 cosmic ray instruments, which indirectly provide energy estimates of ~ 50 eV for the electron beams generating the plasma oscillations⁶.

In Fig. 2 we show the dynamic spectrum of the PWS wideband data from 2015 through early 2020. Fig. 2a shows the same data as in Fig. 1, but with additional mitigation of telemetry errors (see Methods). Fig. 2b shows the same dynamic spectrum but with a different color stretch that shows evidence of a new narrowband signal spanning the entire period of data available between 2017 and 2020. Fig. 2c shows the result of convolving a 1D boxcar filter in time with the dynamic spectrum.

The narrowband signal shown in Fig. 2 constitutes a new class of plasma wave emission in the Voyager spectrum. Unlike previously detected plasma oscillations, its narrower width remains roughly constant at about 0.04 kHz, and it persists for almost three years (barring data dropouts), corresponding to a distance traveled by the spacecraft of about 10 au. The signal-to-noise ratio (SNR) of the narrowband emission is no more than 2 in a single 48 s epoch and requires some degree of averaging to be measured (see Methods). By contrast, previously detected POEs are detectable within individual epochs at the sub-millisecond level with SNRs > 100 , and can vary by more than an order of magnitude in intensity between epochs spaced a few days apart. There is also no evidence of the narrowband signal spreading in frequency or monotonically drifting upwards in frequency. The narrowband plasma wave emission thus appears to be phenomenologically distinct from the shock-generated POEs.

The peak frequency of the narrowband emission vs. time is shown in Fig. 3. The peak frequency was measured by running a modified friends-of-friends (FoF) algorithm¹¹ on the spectrum in Fig. 2b. The modified FoF algorithm returns cluster candidates containing local maxima that are adjacent in time and occur near the same frequency, and the candidate containing the highest S/N corresponds to the frequency time series shown in Fig. 3 (see Methods). A Gaussian process model was fit to the frequency time series using Bayesian regression¹² to obtain a continuous model of the peak frequency vs. time, and is shown in blue in Fig. 3. The dynamic spectrum was

then “de-fluctuated” by aligning the peak frequencies of the narrowband emission to a reference frequency of 3 kHz (see Fig. 4). The de-fluctuated spectrum averaged over all epochs in which the narrowband emission was detected is also shown in Fig. 4. Over a timespan of 70 epochs (or 210 days), the average amplitude of the narrowband emission is 0.06 (in units of $\log_{10}(\text{power})$ relative to the noise baseline) and the root-mean-square (rms) of the noise is 0.005. There is no evidence of the narrowband emission above an rms noise amplitude of 0.005 when the data between the POEs of 2013, 2014, and 2015 are also averaged over 210-day timespans. The de-fluctuated spectrum averaged over the entire duration of the signal shows no evidence of plasma line harmonics above an rms noise threshold of 0.002.

Knowledge of the emission mechanism is required to decisively associate the frequency of the narrowband signal with the plasma frequency (f_p) and hence infer the electron density (n_e). The behavior of the narrowband signal before and after the POE of September 2017 is highly suggestive that its frequency traces the plasma density. The leading edge of the 2017 POE occurs at the same frequency (3.06 kHz) as the narrowband emission prior to the POE’s onset. In mid-September 2017 the plasma frequency increases to 3.15 kHz as the associated shock passes over the spacecraft. During the same period, the frequency of the narrowband emission also increases, before drifting downwards over several months after the POE. The frequency of the narrowband emission is also similar to the plasma frequencies measured from POEs in 2015 and 2016, which are consistent with $n_e \sim 0.11 \text{ cm}^{-3}$. This electron density is consistent with the mean density of the Local Interstellar Cloud estimated from carbon absorption lines in spectra of nearby stars¹³.

The weak, narrowband plasma wave emission could be generated through thermal or suprathermal processes. Thermal density fluctuations with wavelengths longer than the Debye length ($\sim 20 \text{ m}$ in the VLISM) can induce electrostatic oscillations at the plasma frequency, and the intensity of the fluctuations can also be enhanced by suprathermal electrons^{14,15}. Thermal plasma oscillations are routinely observed with incoherent radar scattering in Earth’s ionosphere and have intensities enhanced by energetic photoelectrons^{16,17,18}. In the VLISM, suprathermal electrons might be contributed from inside the heliosphere or at the interface between the solar wind and interstellar plasma, or they might come from a source external to the heliosphere. It’s possible that an anisotropy of low-energy cosmic rays from, e.g., a nearby star could induce plasma oscillations. Any explanation of this nature must account for the emission’s apparent onset about 15 au away from the heliopause and its years-long duration.

An alternative explanation for the narrowband signal is quasi-thermal noise (QTN), which has been routinely observed by plasma wave instruments on Cassini, Galileo, and other Solar System missions¹⁹. QTN is generated by the quasi-thermal motions of electrons in a plasma, resulting in a local electric field measured by the antenna. The QTN voltage spectrum peaks at the local f_p , and its overall shape depends on the antenna properties, with thin antenna longer than

the Debye length required to mitigate shot noise¹⁹. The Voyager antenna, with an effective length of 10 meters and width of 12.5 mm, might be able to detect a marginal peak at f_p in the QTN spectrum, but QTN generally predicts a much broader frequency bandwidth than we observe. A much longer antenna on a future interstellar probe would be capable of robustly detecting QTN and distinguishing QTN from narrowband plasma oscillations.

The peak frequency of the narrowband emission does likely track the plasma frequency, so we use the frequency time series in Fig. 3 to estimate the spectral coefficient of the electron density power spectrum. The power spectrum of electron density fluctuations in the ISM follows a roughly power-law dependence of the form:

$$P_{\delta n_e}(\mathbf{q}) = C_n^2 q^{-\beta}, \quad q_o \leq q \leq q_i \quad (1)$$

where C_n^2 is the spectral coefficient, and q_o and q_i are the outer and inner scales of turbulence²⁰. Scattering measurements from compact radio sources like pulsars have constrained the inner scale of turbulence in the ISM to be between about 100 and 1000 km^{21,22,23}. A recent analysis of electron densities measured with V1 from 2012 through late 2016 showed broad consistency with a Kolmogorov power law ($\beta = 11/3$), but found a higher spectral coefficient at the smallest spatial scales \sim 10s of meters, which may be related to the physical mechanisms mediating turbulence at these scales (e.g., wave instabilities or kinetic Alfvén waves)^{4,24,25}. In the VLISM, turbulence is significantly modified by coronal mass ejections and shocks propagating out of the heliosphere, and may be driven at an outer scale ~ 0.01 pc²⁶, while the inner scale may be related to the ion or electron gyroradii or the Debye length⁴.

The densities inferred from the narrowband emission reveal variations on scales ~ 1 au combined with discrete events on ~ 0.5 au scales produced by shocks originating in the heliosphere. The observed variance of the density fluctuations is directly related to the density power spectrum (Eq. 1) integrated up to 10 au, the largest scale probed in this study (see Methods). We find $C_n^2 \approx 10^{-1.64} \text{ m}^{-20/3}$, considerably larger than the value estimated by Lee & Lee (2019) using earlier Voyager data⁴. The ratio of the rms density fluctuations to the mean density is $\text{rms}(n_e)/\bar{n}_e = 0.0041/0.12 = 0.034$.

In the local ISM, within about 1 kpc probed by pulsar observations, the spectral coefficient for $\beta = 11/3$ is $C_n^2 \approx 10^{-3.5} \text{ m}^{-20/3}$, although scattering observations of pulsars in different regions of the Galactic ISM show C_n^2 ranging from $10^{-5} \text{ m}^{-20/3}$ for underdense regions (e.g., high above the Galactic plane or towards the Galactic anti-center) to $10^2 \text{ m}^{-20/3}$ for overdense regions near the Galactic center or in the spiral arms, where supernova remnants and star-formation regions are more prevalent^{27,28}. The electron density of the local ISM has a scale height of about 1.6 kpc and mean density at mid-plane of 0.015 cm^{-3} ²⁹. Integrating the Kolmogorov wavenumber spectrum up to 10 au with $C_n^2 = 10^{-3.5} \text{ m}^{-20/3}$ yields $\text{rms}(n_e) = 4.8 \times 10^{-4} \text{ cm}^{-3}$, which combined

with $\bar{n}_e = 0.015 \text{ cm}^{-3}$ gives $\text{rms}(n_e)/\bar{n}_e = 0.032$ for the local ISM, very close to our observed value for the VLISM.

Given Voyager's proximity to the heliosphere, solar-origin shocks likely have a significant effect on turbulence in the ambient medium and probably explain why the spectral coefficient is higher than the Kolmogorov value. Magnetic field fluctuations observed by V1 show large magnetic compressibility and significant small-scale fluctuations between 2017 and 2019, including quasi-periodic oscillations in 2017 and multiple pressure pulses in 2018, and the magnetic field fluctuation spectrum also yields power spectral densities higher than the Kolmogorov prediction at the smallest scales probed in that study ($\sim 7 \text{ au}$)³⁰. A similar analysis of the magnetic field data from 2019 has not yet been published, and it would be interesting to see if the magnetic field shows lower levels of compressibility given the smaller density fluctuations that we observe in that time period.

The extremely weak, narrowband plasma wave emission reported here persists over about 10 au of interstellar space traversed by V1. The emission appears to be distinct from shock-generated plasma oscillations that were previously used to measure the local density of plasma outside the heliopause, and it may be generated by thermally or suprathermally excited plasma oscillations. The persistence of the emission through the most recent data published from V1 suggests that it may continue to be detectable. Continued tracking of the emission's frequency, bandwidth, and intensity will likely provide improved constraints on the emission's origin, and make it possible for V1 to quasi-continuously track the electron density distribution of the VLISM along its trajectory. This future work will improve our understanding of the large-scale structure of the VLISM and may reveal the extent of the Sun's role mediating interstellar turbulence.

Methods

Constructing the wideband spectra The V1 PWS wideband receiver measures the voltage difference across the spacecraft antenna terminals at a rate of 28,800 samples s^{-1} for about 48 s to construct a voltage time series that is stored for later transmission to ground. Voltage time series are measured about once a week, although over the course of the mission this time gap varies from about a day to a couple of weeks. The voltage time series are converted into a frequency-time spectrum by the Fourier transform method, which allows tuning of the output spectrum's frequency resolution. To construct the composite dynamic spectra shown in Fig. 1 and Fig. 2, the spectra of the voltage time series were sorted into 3-day long bins and then averaged within each bin. The subsequent time and frequency resolution of the spectrum in Fig. 1 is 3 days and 0.011 kHz, respectively. A lower frequency resolution of 0.02 kHz was used to construct Fig. 2 in order to avoid contamination of the narrowband signal by spectral ringing.

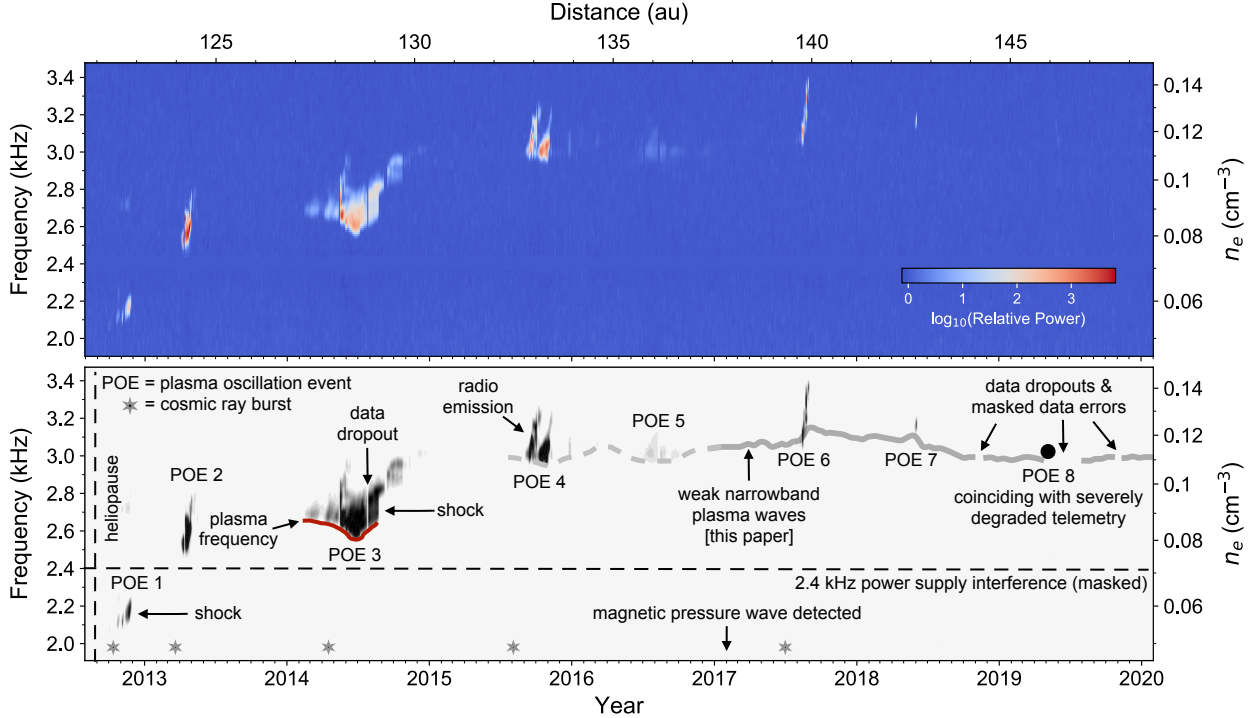


Figure 1: Voyager 1 composite plasma wave spectrum. Top: Frequency-time dynamic spectrum showing all of the Voyager 1 PWS wideband data available since Voyager 1 crossed the heliopause on August 25, 2012. The time resolution of the spectrum is 3 days and the frequency resolution is 0.011 kHz. Each column of pixels corresponds to a 1D spectrum that is the average of all ≈ 48 s long observations that fall within that 3-day time bin. The individual spectra that fall within a given time bin have been equilibrated to the same noise baseline. The 2.4 kHz supply interference line is masked out, and the spectrum is smoothed with a 1D Gaussian smoothing kernel with $\sigma = 0.01$ kHz. Bottom: Schematic showing relevant features in the PWS spectrum, including the locations of previously detected plasma oscillation events (POEs). Two events have direct associations with shocks detected by the magnetometer. A magnetic pressure wave was also detected in early 2017. The lower cutoff frequency of the plasma oscillations corresponds to the local plasma frequency. The approximate times of relativistic electron bursts detected by the cosmic ray instruments are also indicated. The model of the weak, narrowband plasma wave emission presented in this paper is shown in solid gray, and the plasma frequency inferred from POE activity between 2015 and 2017 is shown in dashed gray. A POE detected in June 2019 is also shown as a black circle, but was masked in our analysis because it coincided with a period of severely degraded telemetry performance.

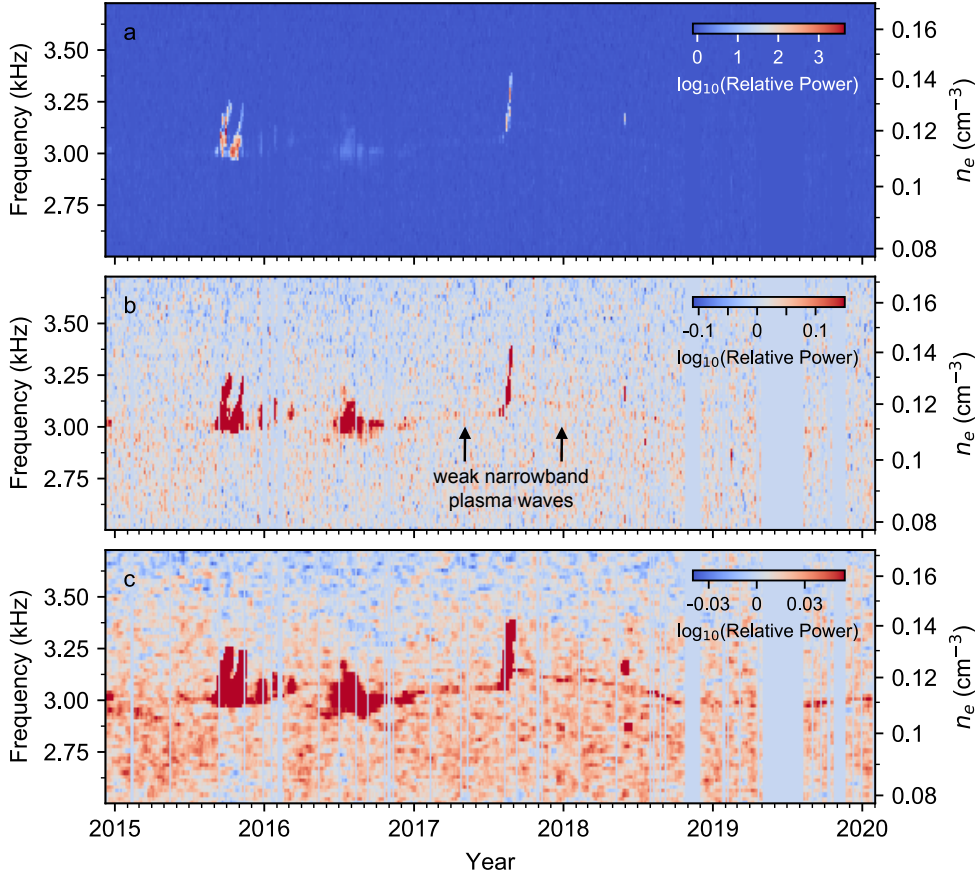


Figure 2: Weak narrowband plasma waves in the Voyager 1 dynamic spectrum. a) Dynamic spectrum showing the Voyager 1 PWS wideband data from December 2014 through January 2020. The spectrum was created using the same methods as Fig. 1, but with a slightly coarser frequency resolution (about 0.02 kHz) to avoid spectral ringing, and without Gaussian smoothing. Epochs contaminated by telemetry errors have been masked out; masked data and data dropouts appear as vertical stripes with zero logarithmic power. b) Same as top panel, but with a different color stretch that extends to 0.16 in logarithmic power. c) Same as top panel but smoothed in time using a 1D boxcar filter and a color stretch extending to a logarithmic power of 0.055.

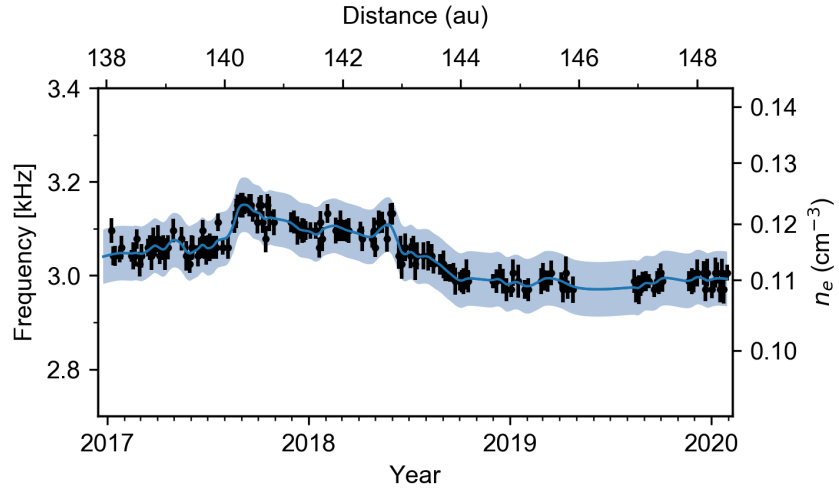


Figure 3: **Peak frequency vs. time of the narrowband plasma wave emission.** The frequencies were extracted by running a friends-of-friends algorithm on the spectrum in Fig. 2b. Error bars represent the rms of the noise fluctuations in each column of Fig. 2b. The blue curve shows the best-fit Gaussian process model and 95% confidence intervals. The density is assumed constant during data dropouts.

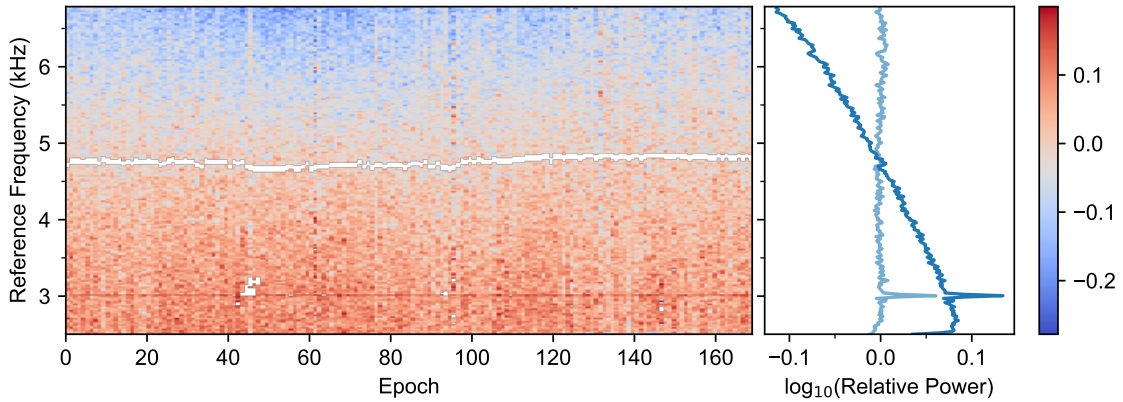


Figure 4: **De-fluctuated dynamic spectrum of the narrowband plasma wave emission.** Epochs shown are between January 2017 and February 2020 when the narrowband plasma wave emission was detected. The peak frequency of the emission was aligned to a reference frequency of 3 kHz. The 4.8 kHz harmonic of the power supply interference line was masked (white) prior to shifting the spectrum. The right-hand panel shows the de-fluctuated spectrum averaged in time with the power-law noise continuum included (dark blue) and with the continuum removed using a second-order polynomial fit to the logarithmic power vs. frequency (light blue). There is no evidence of a plasma line harmonic at 6 kHz.

Due to automatic gain control (AGC), the noise baseline of the voltage time series measured by the wideband receiver varies between observations. To correct for this effect, we equilibrated the noise threshold of the spectra obtained from the voltage time series by subtracting the noise continuum from each spectrum. The 2.4 kHz supply interference line and its harmonics were masked prior to noise equilibration. Our spectra therefore do not represent the absolute electric field intensity and should only be interpreted as the intensity relative to the noise baseline.

There are two main sources of data quality degradation in the V1 wideband spectra. The first is spectral interference that persists throughout the entire timespan since V1 entered the VLISM (and prior): this includes the 2.4 kHz supply interference line and its harmonics, and high-intensity, low-frequency noise that dominates the spectra up to about 1 kHz. We avoided this spectral interference by masking each spectrum at the corresponding frequencies. The second source is degraded telemetry performance that produces bit errors causing short, temporal ($\lesssim 1$ s), wideband bursts that vary in intensity and can take up to all of the frequency band. For most of the interstellar mission, these wideband bursts usually occur just a couple of times per observation, are about 5 kHz wide, and are only up to an order of magnitude more intense than the baseline noise. However, at Voyager’s great distance from the Sun, the signal-to-noise ratio of the telemetry signal arriving at the NASA Deep Space Network (DSN) is increasingly close to the level at which it cannot be decoded. As a result, since 2018 there has been a dramatic increase in the number, frequency bandwidth, and intensity of these bursts, which has been temporarily mitigated by the addition of a fourth antenna to the DSN array. The subsequent decrease in overall data quality had a minimal effect on the 8-yr long composite spectrum shown in Fig. 1 due to its long timespan, and we further reduced the minor effects of these bursts by applying a 1D Gaussian smoothing kernel with $\sigma = 0.01$ kHz to the entire spectrum in Fig. 1.

In order to accurately detect the narrowband signal shown in Fig. 2, we masked the wideband bursts in each 48 s long spectrum before binning and averaging all of the spectra to create the composite dynamic spectrum in Fig. 2. We also ignored altogether individual spectra that are completely contaminated by interference bursts, which corresponds to spectra containing 10 or more bursts, or equivalently, a noise threshold that is more than 5 times the equilibrated noise threshold of the composite spectrum.

Plasma density detection and analysis A modified friends-of-friends (FoF) algorithm¹¹ extracted the plasma frequency (and hence density) time series shown in Fig. 3 from the unsmoothed spectrum of the narrowband signal (see Fig. 2b). The modified FoF algorithm searched for continuous lines in the spectrum by finding all adjacent local maxima within a 0.2 kHz-wide band around a given starting frequency. The line candidates returned by FoF were then sorted by average intensity, and the line with the highest average intensity corresponded to a line in frequency vs. time space that passed through all local maxima containing the new narrowband signal. Outlier maxima picked up by FoF were then excised by calculating a running mean of the line and removing all

points more than 0.04 kHz away from the mean. The “de-fluctuated” spectrum was calculated by shifting the spectrum of the narrowband signal so that the peak frequency of the signal extracted by FoF was aligned to a reference frequency of 3 kHz.

A Gaussian process model was fit to the plasma density time series using the GaussianProcessRegressor module provided by `scikit-learn`¹², with the prior set to a white noise kernel added to a Matern kernel. The Matern kernel takes the form:

$$k(x_i, x_j) = \frac{1}{\Gamma(\nu)2^{\nu-1}} \left(\frac{\sqrt{2\nu}}{l} d(x_i, x_j) \right)^\nu K_\nu \left(\frac{\sqrt{2\nu}}{l} d(x_i, x_j) \right) \quad (2)$$

where K_ν is a modified Bessel function, ν is set to 1 and l is set to 10. The time series of mean, posterior values then gave a continuous temporal model for the frequency of the narrowband emission. In Fig. 3, we show the Gaussian process model and the 95% confidence intervals of the posterior, with the assumption that the density is essentially constant during the large data gaps in late 2019 and 2020. The model is also shown next to previously detected POEs in the bottom panel of Fig. 1, but with the largest data gaps in the density time series indicated.

The variance of electron density fluctuations is directly related to the density fluctuation power spectrum (Eq. 1) integrated over wavenumber $q = 2\pi/L$, where the length scale L is related to the spacecraft speed (3.6 AU/yr). For an outer scale q_o much less than the inner scale q_i , the integrated 3D wavenumber spectrum has the form

$$\text{Var}(n_e) = \frac{2(2\pi)^{4-\beta} C_n^2 l_o^{\beta-3}}{\beta - 3} \approx 3(2\pi)^{1/3} C_n^2 l_o^{2/3}, \quad (3)$$

where $\beta > 3$ and the second approximation is for $\beta = 11/3$. The spectral coefficient C_n^2 for the VLISM was estimated using the observed variance of the density time series and $\beta = 11/3$. Eq. 3 was also used to calculate the density fluctuation variance assuming $C_n^2 = 10^{-3.5}$ for the local ISM.

Data Availability The Voyager 1 data used in this work are archived through the NASA Planetary Data System (<https://pds.nasa.gov>). Data and examples of the PWS data processing algorithms are also available through the University of Iowa Subnode of the PDS Planetary Plasma Interactions Node (<https://space.physics.uiowa.edu/voyager/data/>).

1. D. A. Gurnett, W. S. Kurth, L. F. Burlaga, and N. F. Ness. In Situ Observations of Interstellar Plasma with Voyager 1. *Science*, 341(6153):1489–1492, September 2013. doi: 10.1126/science.1241681.
2. D. A. Gurnett and W. S. Kurth. Plasma densities near and beyond the heliopause from the Voyager 1 and 2 plasma wave instruments. *Nature Astronomy*, 3:1024–1028, November 2019. doi: 10.1038/s41550-019-0918-5.

3. W. S. Kurth and D. A. Gurnett. Observations of a Radial Density Gradient in the Very Local Interstellar Medium by Voyager 2. *ApJL*, 900(1):L1, September 2020. doi: 10.3847/2041-8213/abae58.
4. K. H. Lee and L. C. Lee. Interstellar turbulence spectrum from in situ observations of Voyager 1. *Nature Astronomy*, 3:154–159, January 2019. doi: 10.1038/s41550-018-0650-6.
5. D. A. Gurnett, W. S. Kurth, E. C. Stone, A. C. Cummings, S. M. Krimigis, R. B. Decker, N. F. Ness, and L. F. Burlaga. Precursors To Interstellar Shocks of Solar Origin. *ApJ*, 809(2):121, August 2015. doi: 10.1088/0004-637X/809/2/121.
6. D. A. Gurnett, W. S. Kurth, E. C. Stone, A. C. Cummings, B. Heikkila, N. Lal, S. M. Krimigis, R. B. Decker, N. F. Ness, and L. F. Burlaga. A Foreshock Model for Interstellar Shocks of Solar Origin: Voyager 1 and 2 Observations. *AJ*, 161(1):11, January 2021. doi: 10.3847/1538-3881/abc337.
7. Iver H. Cairns and P. A. Robinson. Theory for low-frequency modulated Langmuir wave packets. *Geophysical Research Letters*, 19(22):2187–2190, November 1992. doi: 10.1029/92GL02632.
8. G. B. Hospodarsky, D. A. Gurnett, W. S. Kurth, M. G. Kivelson, R. J. Strangeway, and S. J. Bolton. Fine structure of Langmuir waves observed upstream of the bow shock at Venus. *JGR*, 99(A7):13363–13372, January 1994. doi: 10.1029/94JA00868.
9. L. F. Burlaga, N. F. Ness, D. A. Gurnett, and W. S. Kurth. Evidence for a Shock in Interstellar Plasma: Voyager 1. *ApJL*, 778(1):L3, November 2013. doi: 10.1088/2041-8205/778/1/L3.
10. T. K. Kim, N. V. Pogorelov, and L. F. Burlaga. Modeling Shocks Detected by Voyager 1 in the Local Interstellar Medium. *ApJL*, 843(2):L32, July 2017. doi: 10.3847/2041-8213/aa7b2b.
11. J. P. Huchra and M. J. Geller. Groups of Galaxies. I. Nearby groups. *ApJ*, 257:423–437, June 1982. doi: 10.1086/160000.
12. F. Pedregosa, G. Varoquaux, A. Gramfort, V. Michel, B. Thirion, O. Grisel, M. Blondel, P. Prettenhofer, R. Weiss, V. Dubourg, J. Vanderplas, A. Passos, D. Cournapeau, M. Brucher, M. Perrot, and E. Duchesnay. Scikit-learn: Machine learning in Python. *Journal of Machine Learning Research*, 12:2825–2830, 2011.
13. Seth Redfield and Ross E. Falcon. The Structure of the Local Interstellar Medium. V. Electron Densities. *ApJ*, 683(1):207–225, August 2008. doi: 10.1086/589230.
14. E. E. Salpeter. Electron Density Fluctuations in a Plasma. *Physical Review*, 120(5):1528–1535, December 1960. doi: 10.1103/PhysRev.120.1528.

15. Francis Perkins and E. E. Salpeter. Enhancement of Plasma Density Fluctuations by Nonthermal Electrons. *Physical Review*, 139(1A):55–62, July 1965. doi: 10.1103/PhysRev.139.A55.
16. J. P. Dougherty and D. T. Farley. A Theory of Incoherent Scattering of Radio Waves by a Plasma. *Proceedings of the Royal Society of London Series A*, 259(1296):79–99, November 1960. doi: 10.1098/rspa.1960.0212.
17. H. C. Carlson, V. B. Wickwar, and G. P. Mantas. Observations of fluxes of suprathermal electrons accelerated by HF excited instabilities. *Journal of Atmospheric and Terrestrial Physics*, 44:1089–1100, December 1982. doi: 10.1016/0021-9169(82)90020-4.
18. Juha Vierinen, Björn Gustavsson, David L. Hysell, Michael P. Sulzer, Phil Perillat, and Erhan Kudeki. Radar observations of thermal plasma oscillations in the ionosphere. *Geophysical Research Letters*, 44(11):5301–5307, June 2017. doi: 10.1002/2017GL073141.
19. N. Meyer-Vernet, K. Issautier, and M. Moncuquet. Quasi-thermal noise spectroscopy: The art and the practice. *Journal of Geophysical Research (Space Physics)*, 122(8):7925–7945, August 2017. doi: 10.1002/2017JA024449.
20. B. J. Rickett. Radio propagation through the turbulent interstellar plasma. *ARA&A*, 28:561–605, January 1990. doi: 10.1146/annurev.aa.28.090190.003021.
21. Steven R. Spangler and Carl R. Gwinn. Evidence for an Inner Scale to the Density Turbulence in the Interstellar Medium. *ApJL*, 353:L29, April 1990. doi: 10.1086/185700.
22. N. D. Ramesh Bhat, James M. Cordes, Fernando Camilo, David J. Nice, and Duncan R. Lorimer. Multifrequency Observations of Radio Pulse Broadening and Constraints on Interstellar Electron Density Microstructure. *ApJ*, 605(2):759–783, April 2004. doi: 10.1086/382680.
23. Barney Rickett, Simon Johnston, Taryn Tomlinson, and John Reynolds. The inner scale of the plasma turbulence towards PSR J1644-4559. *MNRAS*, 395(3):1391–1402, May 2009. doi: 10.1111/j.1365-2966.2009.14471.x.
24. M. Neugebauer. The enhancement of solar wind fluctuations at the proton thermal gyroradius. *JGR*, 80(7):998, March 1975. doi: 10.1029/JA080i007p00998.
25. C. H. K. Chen, C. S. Salem, J. W. Bonnell, F. S. Mozer, and S. D. Bale. Density Fluctuation Spectrum of Solar Wind Turbulence between Ion and Electron Scales. *Phys. Rev. Lett.*, 109(3):035001, July 2012. doi: 10.1103/PhysRevLett.109.035001.
26. L. F. Burlaga, V. Florinski, and N. F. Ness. Turbulence in the Outer Heliosheath. *ApJ*, 854(1):20, February 2018. doi: 10.3847/1538-4357/aaa45a.

27. J. M. Cordes, J. M. Weisberg, D. A. Frail, S. R. Spangler, and M. Ryan. The galactic distribution of free electrons. *Nature*, 354(6349):121–124, November 1991. doi: 10.1038/354121a0.
28. M. A. Krishnakumar, D. Mitra, A. Naidu, B. C. Joshi, and P. K. Manoharan. Scatter Broadening Measurements of 124 Pulsars At 327 Mhz. *ApJ*, 804(1):23, May 2015. doi: 10.1088/0004-637X/804/1/23.
29. Stella Koch Ocker, James M. Cordes, and Shami Chatterjee. Electron Density Structure of the Local Galactic Disk. *ApJ*, 897(2):124, July 2020. doi: 10.3847/1538-4357/ab98f9.
30. Federico Fraternale and Nikolai V. Pogorelov. Waves and turbulence in the very local interstellar medium: From macroscales to microscales. *ApJ*, 906(2):75, Jan 2021. doi: 10.3847/1538-4357/abc88a.

1 Acknowledgements

Authors S.K.O., J.M.C., S.C., and S.R.S. acknowledge support from the National Aeronautics and Space Administration (NASA 80NSSC20K0784). S.K.O., J.M.C., and S.C. also acknowledge support from the National Science Foundation (NSF AAG-1815242) and are members of the NANOGrav Physics Frontiers Center, which is supported by the NSF award PHY-1430284. The research at the University of Iowa was supported by NASA through Contract 1622510 with the Jet Propulsion Laboratory.

2 Author Contributions

S.K.O. conducted the data analysis and wrote the initial draft of the paper. J.M.C., S.C., S.R.S., and S.K.O. are NASA Outer Heliosphere Guest Investigators on the Voyager Interstellar Mission. D.A.G. is the Principal Investigator of the Voyager PWS investigation and W.S.K. is a Co-Investigator of Voyager PWS and is responsible for the initial processing of the data at the University of Iowa. All authors contributed to discussion of the results and comments on the draft.

3 Competing Interests

The authors declare no competing interests.

4 Materials and Correspondence

Correspondence and requests for materials should be directed to S.K.O.